 

# Direct Decomposition of NO into $N_2$ and $O_2$ on C-type Cubic $Y_2O_3$–$ZrO_2$ and $Y_2O_3$–$ZrO_2$–BaO

**Soichiro Tsujimoto, Xiaojing Wang, Toshiyuki Masui, and Nobuhito Imanaka***

Department of Applied Chemistry, Faculty of Engineering, Osaka University, 2-1 Yamadaoka, Suita, Osaka 565-0871

Received December 27, 2010; E-mail: imanaka@chem.eng.osaka-u.ac.jp

Catalytic activities for direct NO decomposition were investigated on C-type cubic $Y_2O_3$–$ZrO_2$ and $Y_2O_3$–$ZrO_2$–BaO prepared by coprecipitation. Introduction of excess oxide anions in the $Y_2O_3$ lattice was achieved by partial substitution of the $Y^{3+}$ sites with $Zr^{4+}$, and high NO decomposition activity was obtained for the $(Y_{0.97}Zr_{0.03})_2O_{3.03}$ catalyst. In addition, the catalytic activity was further enhanced by partial substitution of the $Y^{3+}$ sites in the $Y_2O_3$–$ZrO_2$ solid solution with $Ba^{2+}$, and the $(Y_{0.89}Zr_{0.07}Ba_{0.04})_2O_{3.03}$ catalyst exhibited the highest NO decomposition activity among the samples prepared; NO conversion to $N_2$ reached 90% at 1173 K in the absence of $O_2$ (NO/He atmosphere), and a relatively high conversion ratio was observed even in the presence of $O_2$, $H_2O$, or $CO_2$, compared with the activities of conventional direct NO decomposition catalysts. These results indicate that the C-type cubic $Y_2O_3$–$ZrO_2$–BaO catalyst is a new potential candidate for direct NO decomposition.

Nitrogen oxides ($NO_x$) are not only harmful to human beings, but are also responsible for photochemical smog and acid rain when they are formed in relatively large quantities in the atmosphere. $NO_x$ is a generic term that includes nitrogen monoxide (NO) and nitrogen dioxide ($NO_2$), which are mainly produced by the combustion of fossil fuels such as petroleum in the diesel engines of vehicles and ships, or coke in large-size boilers used in factories. $NO_x$ species in exhaust gases emitted at high temperatures are composed principally of thermodynamically stable NO and a negligible amount of $NO_2$. Accordingly, research should be focused on NO with respect to catalytic $NO_x$ decomposition.

Several NO reduction processes have been proposed for $NO_x$ removal, of which selective catalytic reduction processes employing ammonia or urea have been extensively studied, and have already been practically applied in diesel engines and large-scale boilers.[1] In these processes, high efficiency for NO decomposition has been realized under various conditions and the reaction process is stable at high temperatures. However, separate specialized equipment is necessary to supply the reducing agents and secure control is necessary, due to the toxicity of ammonia.

In contrast to processes employing ammonia or urea, direct catalytic decomposition of NO into $N_2$ and $O_2$ ($2NO \rightarrow N_2 + O_2$) is the most ideal route for $NO_x$ removal, because no reductants are required and no special equipment is necessary. A number of materials, such as zeolites,[2] perovskites,[3–5] and other mixed-oxides,[6–14] have been reported as active catalysts for direct NO decomposition. However, the NO decomposition activity of these conventional catalysts is significantly decreased in the presence of $O_2$, due to the strong adsorption of $O_2$ on the surface of the catalysts.

In contrast, we have elucidated that a catalyst based on C-type cubic rare earth oxide can exhibit higher activity for direct NO decomposition than that of conventional perovskite-type catalysts in the presence of $O_2$.[14–16] Rare earth oxides can form three types of crystal structures, A- (hexagonal), B- (monoclinic), and C-type (cubic), according to the ionic size of the respective rare earth element.[17] Among these, the lattice volume of individual rare earth oxides increase in the order of A-type < B-type < C-type, and the C-type cubic structure has the largest interstitial open space. It has been generally accepted that large open spaces in a catalyst play an important role in the direct NO decomposition, and for this reason the C-type cubic rare earth oxide is suitable as a direct NO removal catalyst. Furthermore, in our previous work, we found that incorporation of excess oxide anions into the C-type cubic lattice is also effective for enhancing direct NO decomposition.[13] Accordingly, the control of lattice defects is carried out by partial substitution of trivalent rare earth cations with $Zr^{4+}$ ions.

In some conventional $NO_x$ storage catalysts, it has been reported that alkaline and alkaline earth metal ions have high $NO_x$ storage properties, of which $Ba^{2+}$ is a well known $NO_x$ storage species.[18] Accordingly, the additional introduction of $Ba^{2+}$ into the C-type cubic lattice of the catalyst should accelerate NO adsorption on the surface and promote activity for NO decomposition.

In the present study, $Y_2O_3$, which is a thermally and chemically stable C-type cubic oxide, was selected as the fundamental material, and a fraction of the $Y^{3+}$ sites were substituted with $Zr^{4+}$ and $Ba^{2+}$ to optimize the amount of oxide anion vacancies in the lattice for effective direct NO decomposition.

## Experimental

The C-type cubic $Y_2O_3$–$ZrO_2$ and $Y_2O_3$–$ZrO_2$–BaO catalysts were synthesized by coprecipitation. A stoichiometric mixture of 1 mol dm$^{-3}$ $Y(NO_3)_3$, 0.1 mol dm$^{-3}$ $ZrO(NO_3)_2$, and 0.1 mol dm$^{-3}$ $Ba(NO_3)_2$ aqueous solutions was added to a 1.0

Published on the web July 2, 2011; doi:10.1246/bcsj.20100360

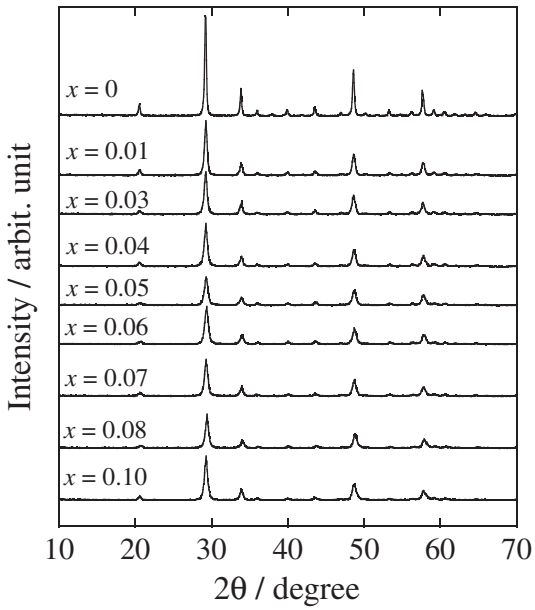


**Figure 1.** XRD patterns of the $(Y_{1-x}Zr_x)_2O_{3+x}$ $(0 \le x \le 0.10)$ catalysts.

mol $dm^{-3}$ ammonium carbonate solution cooled by an ice bath with stirring, and the total amount of cations was adjusted to be 10 mmol. The pH of the mixture was adjusted to 10 by the dropwise addition of ammonia solution. After stirring for 6 h, the resulting precipitate was collected by filtration, washed several times with deionized water, and then dried at 353 K for 6 h. The powder was then ground in an agate mortar and finally calcined at 1173 K in air for 2 h.

The catalysts were characterized using X-ray powder diffraction (XRD; Rigaku Multiflex) with Cu K$\alpha$ radiation. XRD patterns were recorded in the $2\theta$ range from 10 to 70°. The sample compositions were analyzed by X-ray fluorescence spectrometry (XRF; Rigaku, ZSX-100e) and the specific surface area was measured by the BET (Brunauer–Emmett–Teller) method using nitrogen adsorption at 77 K with a Micromeritics Tristar 3000 adsorption analyzer.

The NO decomposition reaction was carried out in a conventional fixed-bed flow reactor with a 10 mm diameter quartz glass tube. A gas mixture of 1.0 vol% NO and He (balance) was fed at a rate of 10 $cm^3$ $min^{-1}$ over 0.5 g of catalyst. The $W/F$ ratio, where $W$ and $F$ are the catalyst weight and gas flow rate, respectively, was adjusted to be 3.0 g s $cm^{-3}$. The gas composition was analyzed using a gas chromatograph (Shimadzu GC-8A) with a thermal conductivity detector (TCD), a molecular sieve 5A column for NO, $N_2$, and $O_2$, and a Polapac-Q column for $N_2O$ separation. The activity of each catalyst was evaluated in terms of NO conversion to $N_2$.

The effect of the presence of $O_2$, $H_2O$, or $CO_2$ was measured by mixing each gas species with the reactant gas. The concentrations of the additional gases and NO were controlled by changing the feed rate of He as the balance gas to maintain a constant total flow rate of reactants at 10 $cm^3$ $min^{-1}$.

## Results and Discussion

Figure 1 shows XRD patterns of the $(Y_{1-x}Zr_x)_2O_{3+x}$ catalysts. All the diffraction patterns can be assigned to C-type cubic rare earth oxides, and no crystalline impurities were observed. Figure 2 shows the effect of the $Zr^{4+}$ content on the $(Y_{1-x}Zr_x)_2O_{3+x}$ lattice parameters estimated from the diffraction angles. The ionic sizes of $Y^{3+}$ and $Zr^{4+}$ with sixfold coordination are 0.1040[19] and 0.0860 nm,[19] respectively. When the smaller $Zr^{4+}$ occupies the lattice position of $Y^{3+}$ in $Y_2O_3$, the lattice parameter decreases monotonically with increasing of $Zr^{4+}$ content. The results indicate that C-type cubic solid solutions were successfully formed for all samples. The catalyst compositions, as determined using XRD, and the BET surface area of the $(Y_{1-x}Zr_x)_2O_{3+x}$ catalysts are summarized in Table 1. The BET specific surface area was almost doubled by the introduction of $Zr^{4+}$ into the $Y_2O_3$ lattice.

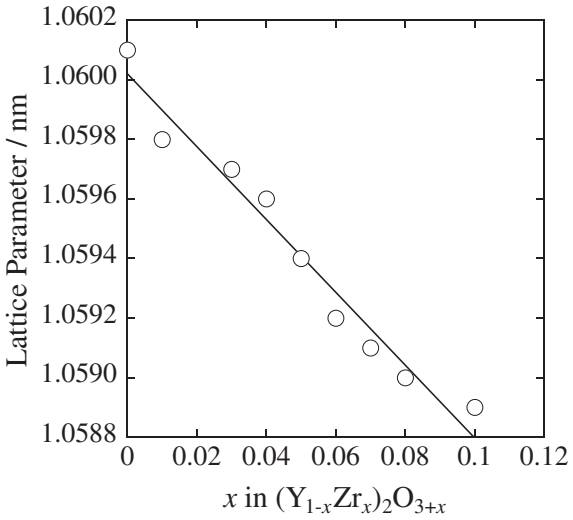


**Figure 2.** Dependence of the lattice parameter on the concentration of $Zr^{4+}$ in the $(Y_{1-x}Zr_x)_2O_{3+x}$ $(0 \le x \le 0.10)$ system.

**Table 1.** Composition and BET Surface Area of the $(Y_{1-x}Zr_x)_2O_{3+x}$ Catalysts

| Sample | BET surface area/$m^2$ $g^{-1}$ |
|---|---|
| $Y_2O_3$ | 15.0 |
| $(Y_{0.99}Zr_{0.01})_2O_{3.01}$ | 31.0 |
| $(Y_{0.97}Zr_{0.03})_2O_{3.03}$ | 32.2 |
| $(Y_{0.96}Zr_{0.04})_2O_{3.04}$ | 33.2 |
| $(Y_{0.95}Zr_{0.05})_2O_{3.05}$ | 33.3 |
| $(Y_{0.94}Zr_{0.06})_2O_{3.06}$ | 32.6 |
| $(Y_{0.93}Zr_{0.07})_2O_{3.07}$ | 29.9 |
| $(Y_{0.92}Zr_{0.08})_2O_{3.08}$ | 29.4 |
| $(Y_{0.90}Zr_{0.10})_2O_{3.10}$ | 28.7 |

The dependence of NO conversion into $N_2$ at 1173 K on the $Zr^{4+}$ concentration in the $(Y_{1-x}Zr_x)_2O_{3+x}$ catalysts is presented in Figure 3. The activity for NO decomposition gradually increased with $Zr^{4+}$ content. However, an excess amount of $Zr^{4+}$ beyond the optimum concentration caused a decrease in the catalytic activity, which was probably due to an excessive reduction in the amount of interstitial open space in the catalyst. As a result, the highest catalytic activity was obtained for the $(Y_{0.97}Zr_{0.03})_2O_{3.03}$ catalyst, on which the $N_2$ yield attained was 60%.

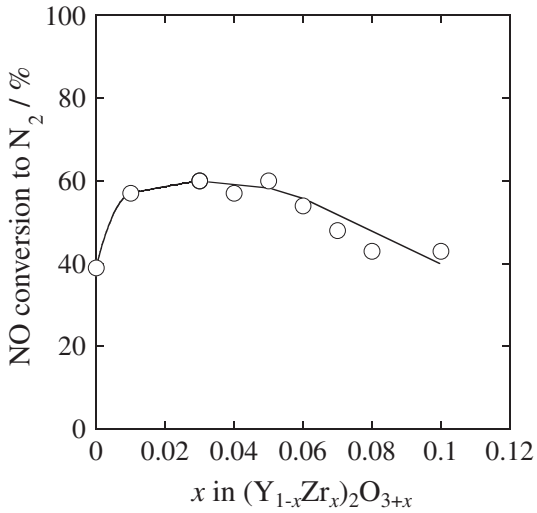


**Figure 3.** Dependence of NO conversion into $N_2$ at 1173 K on the $Zr^{4+}$ concentration in the $(Y_{1-x}Zr_x)_2O_{3+x}$ catalysts (NO: 1 vol %, He; balance, $W/F = 3.0\,g\,s\,cm^{-3}$).

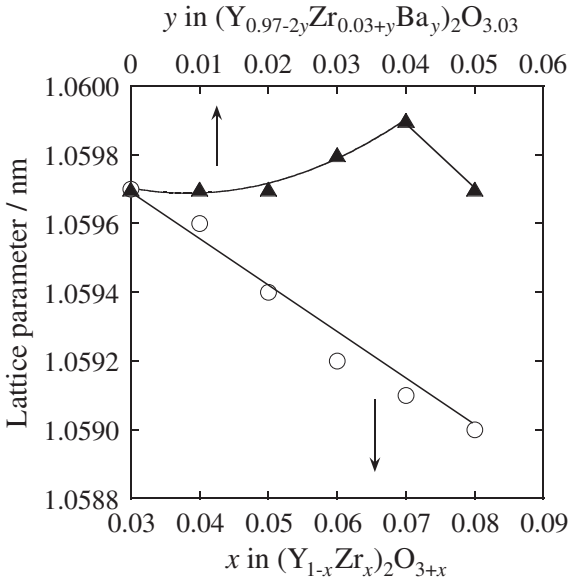


**Figure 5.** Dependence of the lattice parameter on the concentration of $Zr^{4+}$ in $(Y_{1-x}Zr_x)_2O_{3+x}$ ($0.03 \le x \le 0.08$) (○), and $Ba^{2+}$ in $(Y_{0.97-2y}Zr_{0.03+y}Ba_y)_2O_{3.03}$ ($0 \le y \le 0.05$) (▲).

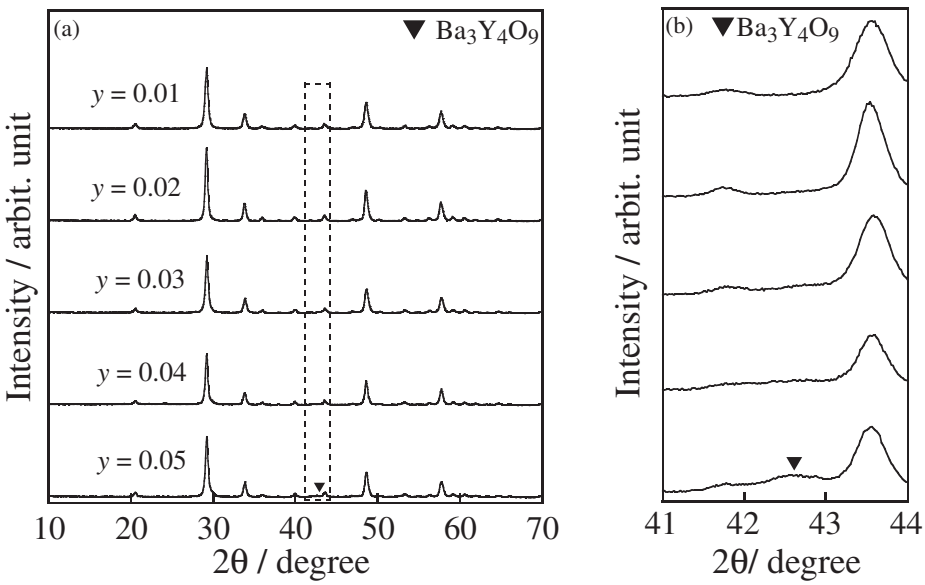


**Figure 4.** XRD patterns of the $(Y_{0.97-2y}Zr_{0.03+y}Ba_y)_2O_{3.03}$ catalysts ($0.01 \le y \le 0.05$) in the $2\theta$ range from (a) 10 to 70°, and (b) 41 to 44°.

The additional introduction of $Ba^{2+}$ should accelerate direct NO decomposition. However, incorporation of divalent $Ba^{2+}$ ions into the $(Y_{0.97}Zr_{0.03})_2O_{3.03}$ lattice produces oxide anion vacancies that counteract the excess oxide anions produced by $Zr^{4+}$ doping. Therefore, additional doping with $Ba^{2+}$ requires further introduction of $Zr^{4+}$ to maintain the optimized open space. In this study, $(Y_{0.97-2y}Zr_{0.03+y}Ba_y)_2O_{3.03}$ catalysts were prepared, in which the same amount of $Ba^{2+}$ and $Zr^{4+}$ was codoped into $(Y_{0.97}Zr_{0.03})_2O_{3.03}$ to maintain the amount of oxide anions in the lattice, and their catalytic activities were evaluated.

Figure 4 shows XRD patterns of the $(Y_{0.97-2y}Zr_{0.03+y}Ba_y)_2O_{3.03}$ catalysts ($0.01 \le y \le 0.05$). A single phase of the C-type cubic rare earth oxide structure was successfully obtained for samples with $0.01 \le y \le 0.04$, whereas $Ba_3Y_4O_9$ was observed as a secondary impurity phase for $(Y_{0.87}Zr_{0.08}Ba_{0.05})_2O_{3.03}$. Figure 5 shows the dependence of the lattice constant on the concentration of $Zr^{4+}$ ($x$) in $(Y_{1-x}Zr_x)_2O_{3+x}$ ($0.03 \le x \le 0.08$) and $Ba^{2+}$ ($y$) in $(Y_{0.97-2y}Zr_{0.03+y}Ba_y)_2O_{3.03}$ ($0 \le y \le 0.05$). In contrast to the results for $(Y_{1-x}Zr_x)_2O_{3+x}$, the lattice parameter of $(Y_{0.97-2y}Zr_{0.03+y}Ba_y)_2O_{3.03}$ ($0 \le y \le 0.05$) gradually increased with the $y$ value, because the same amount of $Zr^{4+}$ and $Ba^{2+}$ occupied the lattice position of $Y^{3+}$ in the $(Y_{0.97}Zr_{0.03})_2O_{3.03}$ lattice, and the ionic size of $Ba^{2+}$ with six coordination number (0.149 nm[19]) is considerably larger than those of $Y^{3+}$ and $Zr^{4+}$.

**Table 2.** Composition and BET Surface Area of the $(Y_{0.97-2y}Zr_{0.03+y}Ba_y)_2O_{3.03}$ Catalysts

| Sample | BET surface area/$m^2\,g^{-1}$ |
|---|---|
| $(Y_{0.97}Zr_{0.03})_2O_{3.03}$ | 32.2 |
| $(Y_{0.95}Zr_{0.04}Ba_{0.01})_2O_{3.03}$ | 27.2 |
| $(Y_{0.93}Zr_{0.05}Ba_{0.02})_2O_{3.03}$ | 20.4 |
| $(Y_{0.91}Zr_{0.06}Ba_{0.03})_2O_{3.03}$ | 20.3 |
| $(Y_{0.89}Zr_{0.07}Ba_{0.04})_2O_{3.03}$ | 21.9 |
| $(Y_{0.87}Zr_{0.08}Ba_{0.05})_2O_{3.03}$ | 19.4 |

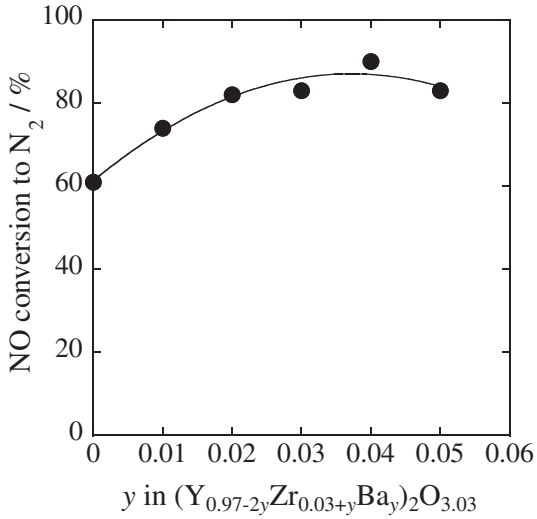


**Figure 6.** Dependence of NO conversion into $N_2$ at 1173 K on the composition of the $(Y_{0.97-2y}Zr_{0.03+y}Ba_y)_2O_{3.03}$ catalysts (NO: 1 vol %, He; balance, $W/F = 3.0\,g\,s\,cm^{-3}$).

However, $Ba_3Y_4O_9$ was separated as a secondary phase in $(Y_{0.87}Zr_{0.08}Ba_{0.05})_2O_{3.03}$ and only the $Zr^{4+}$ ions were dissolved into the lattice. As a result, the lattice parameter became smaller than that of $(Y_{0.89}Zr_{0.07}Ba_{0.04})_2O_{3.03}$. These results indicate that the solubility limit for $(Y_{0.97-2y}Zr_{0.03+y}Ba_y)_2O_{3.03}$ to form a single phase of C-type cubic structure is $y = 0.04$. The catalyst composition and BET surface area of the $(Y_{0.97-2y}Zr_{0.03+y}Ba_y)_2O_{3.03}$ catalysts are summarized in Table 2; the BET specific surface area was decreased by the introduction of $Ba^{2+}$ into the $(Y_{0.97}Zr_{0.03})_2O_{3.03}$ lattice.

Figure 6 shows the dependence of NO conversion into $N_2$ at 1173 K on the composition of the $(Y_{0.97-2y}Zr_{0.03+y}Ba_y)_2O_{3.03}$ catalysts. The catalytic activity of the single phase C-type cubic structure ($0 \le y \le 0.04$) steadily increased with the $y$ value, and the highest catalytic activity was obtained for the $(Y_{0.89}Zr_{0.07}Ba_{0.04})_2O_{3.03}$ composition, which is the solid solubility limit for $Ba^{2+}$ in $(Y_{0.97-2y}Zr_{0.03+y}Ba_y)_2O_{3.03}$. The $N_2$ yield on this catalyst was 90%. In contrast, the catalytic activity of the $(Y_{0.87}Zr_{0.08}Ba_{0.05})_2O_{3.03}$ catalyst decreased, due to the appearance of the secondary $Ba_3Y_4O_9$ phase. Although $Ba_3Y_4O_9$ exhibits catalytic activity for direct NO decomposition,[20] the activity is less than that of $(Y_{0.93}Zr_{0.05}Ba_{0.02})_2O_{3.03}$.

Figure 7 shows the temperature dependence of NO conversion and the yield of $N_2$ and $O_2$ for the $(Y_{0.89}Zr_{0.07}Ba_{0.04})_2O_{3.03}$ catalyst. NO decomposition activity appeared from 823 K, and the NO conversion, $N_2$ yield, and $O_2$ yield increased monotonically with reaction temperature. The

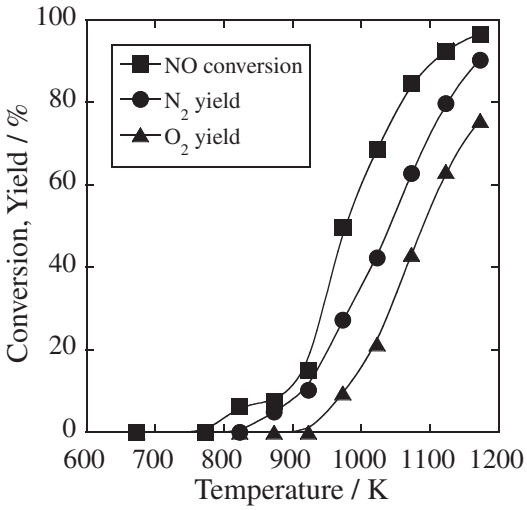


**Figure 7.** Temperature dependence of NO conversion (■) and yield of $N_2$ (●) and $O_2$ (▲) over the $(Y_{0.89}Zr_{0.07}Ba_{0.04})_2O_{3.03}$ catalyst (NO: 1 vol %, He; balance, $W/F = 3.0\,g\,s\,cm^{-3}$).

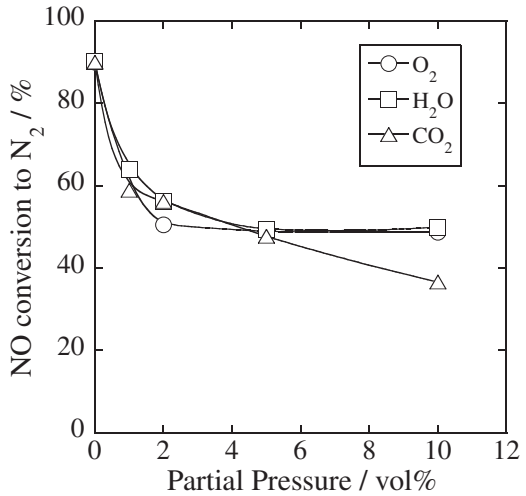


**Figure 8.** Effect of the presence of $O_2$ (○), $H_2O$ (□), or $CO_2$ (△) on the $N_2$ yield over the $(Y_{0.89}Zr_{0.07}Ba_{0.04})_2O_{3.03}$ catalyst at 1173 K (NO: 1 vol %, He; balance, $W/F = 3.0\,g\,s\,cm^{-3}$).

formation of $N_2O$ was not detected between 400 and 900 °C. When the reaction proceeds stoichiometrically, the $N_2$ yield should be equivalent to the $O_2$ yield, however the $O_2$ yield was lower than that of $N_2$. Similar results have been reported in a number of studies,[4,5,12–14] and the formation of $NO_2$ was suggested as the cause.

A significant issue of conventional catalysis for direct NO decomposition is that the activity decreases in the presence of $O_2$. In addition, not only $O_2$ but also $H_2O$ and $CO_2$ appear in exhaust gases from fixed sources. Therefore, the effect of the presence of $O_2$, $H_2O$, or $CO_2$ on the $N_2$ yield over the $(Y_{0.89}Zr_{0.07}Ba_{0.04})_2O_{3.03}$ catalyst at 1173 K was also examined, and the results are presented in Figure 8. In the presence of $O_2$, the $N_2$ yield decreased from 90 to 50% until the content reached 2 vol %, but became almost constant in the range from

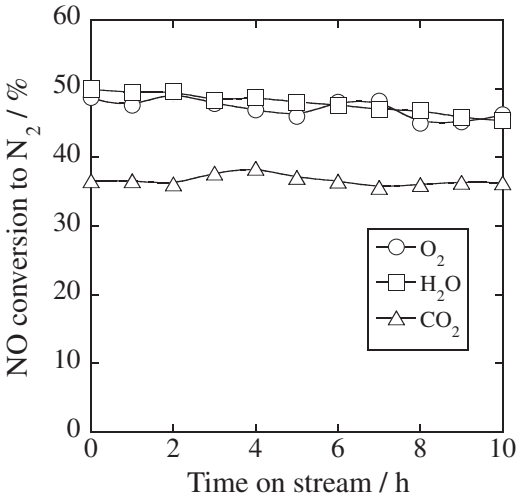


**Figure 9.** Effect of the presence of 10 vol % $O_2$ (○), $H_2O$ (□), or $CO_2$ (△) on the $N_2$ yield over the $(Y_{0.89}Zr_{0.07}Ba_{0.04})_2O_{3.03}$ catalyst at 1173 K as a function of time on stream (NO: 1 vol %, He; balance, $W/F = 3.0\,g\,s\,cm^{-3}$).

2 to 10 vol %. As a result, NO decomposition activity as high as 50% was maintained, even in the presence of 10 vol % $O_2$. Even at 1073 K, the conversion ratio in the presence of 10 vol % $O_2$ was 28% on the $(Y_{0.89}Zr_{0.07}Ba_{0.04})_2O_{3.03}$ catalyst, which is over two times higher than that for $La_{0.7}Ba_{0.3}Mn_{0.8}In_{0.2}O_3$ (12%).[4] A similar trend of decreasing NO decomposition activity was also observed in the presence of $H_2O$. The $N_2$ yield was decreased to 50% when the concentration of water vapor reached 5 vol % or more.

In contrast, the effect of $CO_2$ on the NO decomposition activity was relatively larger than that for $O_2$ and $H_2O$, and the $N_2$ yield monotonically decreased with the increase in the partial pressure of $CO_2$. $CO_2$ is acidic, so that adsorption of $CO_2$ on $Ba^{2+}$ sites on the surface of the catalyst will inhibit the adsorption of NO onto the open space sites of the catalyst. However, on the $(Y_{0.89}Zr_{0.07}Ba_{0.04})_2O_{3.03}$ catalyst, a high $N_2$ yield was sustained at 47% even in the presence of 5 vol % $CO_2$, which is significantly higher than that for the $Ba_{0.8}La_{0.2}Mn_{0.8}Mg_{0.2}O_3$ (20% at 1123 K)[21] and $La_{0.8}Sr_{0.2}CoO_3$ (10% at 1073 K) catalysts.[22]

Furthermore, the stability of the catalysts for direct NO decomposition activity with time-on-stream was evaluated for the $(Y_{0.89}Zr_{0.07}Ba_{0.04})_2O_{3.03}$ catalyst in the presence of 10 vol % $O_2$, $H_2O$, or $CO_2$ at 1173 K. As shown in Figure 9, the catalytic activity was not deactivated during the 10 h run in the presence of each interfering gas, suggesting that the present $(Y_{0.89}Zr_{0.07}Ba_{0.04})_2O_{3.03}$ catalyst was stable in a long period of operation. In addition, the NO decomposition activity was recovered when the catalytic test was carried out again in the absence of the coexisting gases (1 vol % NO/He), and the XRD pattern of the $(Y_{0.89}Zr_{0.07}Ba_{0.04})_2O_{3.03}$ catalyst was the same before and after the reactions. These results indicate that the decrease in NO decomposition activity is caused by the adsorption of $O_2$, $H_2O$, or $CO_2$ on the catalyst, and the negative effects of $O_2$, $H_2O$, or $CO_2$ are not permanent.

## Conclusion

C-type cubic $Y_2O_3$–$ZrO_2$–BaO catalysts, in which the $Y^{3+}$ site is partially substituted with $Zr^{4+}$ and $Ba^{2+}$ to control the open interstitial space in the lattice, were found to exhibit high catalytic activity for direct NO decomposition. The catalytic activity was significantly enhanced by the introduction of $Zr^{4+}$ and $Ba^{2+}$, and the highest catalytic activity was obtained for $(Y_{0.89}Zr_{0.07}Ba_{0.04})_2O_{3.03}$. It is noteworthy that the catalytic activity was maintained with a high conversion ratio even in the presence of $O_2$, $H_2O$, or $CO_2$. Therefore, the $(Y_{0.89}Zr_{0.07}Ba_{0.04})_2O_{3.03}$ catalyst is expected to be a new potential candidate for a direct NO decomposition catalyst.

This research was supported by the Industrial Technology Research Grant Program '08 (Project ID: 08B42001a) from the New Energy and Industrial Technology Development Organization (NEDO) of Japan, and by the Steel Industry Foundation for the Advancement of Environmental Protection Technology (SEPT).

## References

1 Z. Liu, S. I. Woo, *Catal. Rev.* **2006**, *48*, 43.
2 M. Iwamoto, H. Yahiro, K. Tanda, N. Mizuno, Y. Mine, S. Kagawa, *J. Phys. Chem.* **1991**, *95*, 3727.
3 Y. Teraoka, T. Harada, S. Kagawa, *J. Chem. Soc., Faraday Trans.* **1998**, *94*, 1887.
4 T. Ishihara, M. Ando, K. Sada, K. Takiishi, K. Yamada, H. Nishiguchi, Y. Takita, *J. Catal.* **2003**, *220*, 104.
5 H. Iwakuni, Y. Shinmyou, H. Yano, H. Matsumoto, T. Ishihara, *Appl. Catal., B* **2007**, *74*, 299.
6 M. Haneda, Y. Kintaichi, N. Bion, H. Hamada, *Appl. Catal., B* **2003**, *46*, 473.
7 S. Xie, G. Mestl, M. P. Rosynek, J. H. Lunsford, *J. Am. Chem. Soc.* **1997**, *119*, 10186.
8 Z. Liu, J. Hao, L. Fu, T. Zhu, *Appl. Catal., B* **2003**, *44*, 355.
9 Y. Teraoka, K. Torigoshi, H. Yamaguchi, T. Ikeda, S. Kagawa, *J. Mol. Catal. A: Chem.* **2000**, *155*, 73.
10 S. Iwamoto, R. Takahashi, M. Inoue, *Appl. Catal., B* **2007**, *70*, 146.
11 H. Iwakuni, Y. Shinmyou, H. Matsumoto, T. Ishihara, *Bull. Chem. Soc. Jpn.* **2007**, *80*, 2039.
12 T. Ishihara, Y. Shinmyou, K. Goto, N. Nishiyama, H. Iwakuni, H. Matsumoto, *Chem. Lett.* **2008**, *37*, 318.
13 H. Masaki, T. Masui, N. Imanaka, *J. Alloys Compd.* **2008**, *451*, 406.
14 N. Imanaka, T. Masui, H. Masaki, *Adv. Mater.* **2007**, *19*, 3660.
15 N. Imanaka, T. Masui, *Chem. Rec.* **2009**, *9*, 40.
16 S. Tsujimoto, K. Mima, T. Masui, N. Imanaka, *Chem. Lett.* **2010**, *39*, 456.
17 G. Adachi, N. Imanaka, *Chem. Rev.* **1998**, *98*, 1479.
18 B. Westerberg, E. Fridell, *J. Mol. Catal. A: Chem.* **2001**, *165*, 249.
19 R. D. Shannon, *Acta Crystallogr., Sect. A* **1976**, *32*, 751.
20 K. Goto, H. Matsumoto, T. Ishihara, *Top. Catal.* **2009**, *52*, 1776.
21 H. Iwakuni, Y. Shinmyou, H. Yano, K. Goto, H. Matsumoto, T. Ishihara, *Bull. Chem. Soc. Jpn.* **2008**, *81*, 1175.
22 Y. Teraoka, K. Torigoshi, S. Kagawa, *Bull. Chem. Soc. Jpn.* **2001**, *74*, 1161.